Impacts of land cover changes on biogenic emission and its contribution to ozone and secondary organic aerosol in China

Jinlong Ma[1], Shengqiang Zhu[1], Siyu Wang[1], Peng Wang[2,3,4*], Jianmin Chen[1], Hongliang Zhang[1,3,4*]

[1]Shanghai Key Laboratory of Atmospheric Particle Pollution and Prevention, Department of Environmental Science and Engineering, Fudan University, Shanghai, China
[2]CMA-FDU Joint Laboratory of Marine Meteorology, Shanghai 200438, China
[3]Institute of Eco-Chongming (IEC), Shanghai 200062, China
[4]IRDR ICoE on Risk Interconnectivity and Governance on Weather/Climate Extremes Impact and Public Health, Fudan University, Shanghai, China

Correspondence to: Peng Wang (w_peng@fudan.edu.cn); Hongliang Zhang (zhanghl@fudan.edu.cn)

Abstract. The greening impacts in China from 2000 to 2017 led to an increase in vegetated areas and thus enhanced biogenic volatile organic compounds (BVOC) emissions. BVOCs are regarded as important precursors for ozone (O_3) and secondary organic aerosol (SOA). As a result, accurate estimation of BVOC emissions is critical to understand their impacts on air quality. In this study, Model of Emissions of Gases and Aerosols from Nature (MEGAN) v2.1 was used to investigate the impact of different leaf area index (LAI) and land cover (LC) datasets on BVOC emissions in China in 2016 and the effects on O_3 and SOA were evaluated based on the Community Multiscale Air Quality Modelling System (CMAQ). Three LAI satellite datasets of the Global LAnd Surface Satellite (GLASS), the Moderate Resolution Imaging Spectroradiometer (MODIS) MOD15A2H version 6 (MOD15), and the Copernicus Global Land Service (CGLS), as well as three LC satellite datasets of the MODIS MCD12Q1 LC products, the Copernicus Climate Change Service (C3S) LC products, and the CGLS LC products were used in five parallel experiments (cases: C1-C5). Results show that changing LAI and LC datasets of the model input has an impact on BVOC estimations. BVOC emissions in China range from 25.42 to 37.39 Tg in 2016 and are mainly concentrated in central and south-eastern China. Changing the LC inputs for the MEGAN model has a more significant difference in BVOC estimates than using different LAI datasets. The combination of C3S LC and GLASS LAI performs better in the CMAQ model, indicating that it is the better choice for BVOC estimations in China. Among all cases, the highest contribution of BVOCs to O_3 and SOA can reach 12 ppb and 9.8 μg m^{-3}, respectively. Changing the MEGAN inputs further impacts the concentrations of O_3 and SOA, especially changing LC datasets. The relative difference between MCD12Q1 LC and C3S LC is over 52% and 140% in O_3 and biogenic SOA (BSOA) in central and eastern China. Overall, the BSOA difference is mainly attributed to the isoprene SOA (ISOA), a major contributor to BSOA. The relative differences in ISOA between different cases are up to 160% in eastern China. Therefore, our results suggest that the uncertainties in MEGAN inputs should be fully considered in future O_3 and SOA simulations.

1 Introduction

Volatile organic compounds (VOCs) from both natural and anthropogenic sources play important roles in the formation of ozone (O_3) and secondary components of fine particulate matter ($PM_{2.5}$) in addition to their adverse health effects (Volkamer et al., 2006;Laothawornkitkul et al., 2009;Calfapietra et al., 2013;Zhao et al., 2021). Globally, biogenic VOCs from vegetations (BVOCs) are the dominant contributor (with ~90% contribution) to VOCs (Fehsenfeld et al., 1992;Guenther et al., 1995). Isoprene, monoterpenes, and sesquiterpenes are major BVOC species (Guenther et al., 2006;Wang et al., 2018a) with high photo-chemical reactivity with O_3, hydroxyl radical (OH), and nitrate radical (NO_3). In addition, changes in BVOC emissions also apparently alter the concentrations of key pollutants that affect the climate. In particular, O_3, methane (CH_4) and aerosols. O_3 and CH_4 can warm the climate, while the aerosols have a cooling effect by scattering solar radiation (Unger, 2014a, b). Consequently, the studies of BVOC emissions and their effects on air quality and climate are of vital significance.

The Model of Emissions of Gases and Aerosols from Nature (MEGAN) is a widely used (Guenther et al., 2012;Zhao et al., 2016;Emmerson et al., 2018) model to quantify BVOC emissions in different spatial scales (Guenther et al., 1995;Sindelarova et al., 2014;Zhang et al., 2017;Jiang et al., 2019a;Wang et al., 2021). Global annual inventories of the isoprene emission range from 500 to 750 Tg yr^{-1} (Guenther et al., 2006) and those of monoterpene emissions range from 74.4-157 Tg yr^{-1} (Guenther et al., 2012;Messina et al., 2016). BVOC emissions also have been estimated in China by various studies and the results showed that isoprene emissions were 7.17-29.30 Tg yr^{-1} and monoterpene emissions were 2.83-5.60 Tg yr^{-1} (Guenther et al., 2006;Fu and Liao, 2012;Li et al., 2020). The model determined the vegetation types according to model inputs and then use the activity factor multiplied with the emission factor to calculate emissions for each vegetation type (Guenther et al., 2012). However, there are considerable uncertainties in BVOC estimations due to incomplete information on model inputs, activity factors, and emission factors (Situ et al., 2014;Guenther et al., 2012). Those factors can influence the accuracy of estimations and further result in uncertainties on O_3 and SOA. Therefore, it is necessary to quantify the influence of those factors and determine the bias in BVOC emissions.

Land cover (LC), including leaf area index (LAI) and plant function types (PFTs) fractions, is a major factor affecting the BVOC emissions in the MEGAN model (Guenther et al., 2006;Pfister et al., 2008;Guenther et al., 2012). There are many LAI and LC products generated by various satellite sensors with different process methods, spatial and temporal resolutions. These products show discrepancies in biomass distributions and PFTs fractions which can enlarge bias in BVOC estimations (Leung et al., 2010;Wang et al., 2020b;Opacka et al., 2021). Guenther et al. (2006) reported that differences in isoprene emissions could be 24% and 29% due to changing PFTs and LAI, respectively. Pfister et al. (2008) found that differences in BVOC emissions were more significant on a regional scale than global by employing three different PFTs and LAI databases to drive the MEGAN model. Wang et al. (2018a) showed that the differences in BVOC estimations were 35.5% and 22.8% as a result of changing PFTs and LAI, respectively. China is a typical greening country across the world with the forest area of 22.96%

65   in 2018 (NFGA, 2019), contributing large annual BVOC emissions to the world (Opacka et al., 2021), and thus reasonable comparisons in LAI and LC satellite products are essential for better understanding China BVOC emissions.

Contributions of BVOCs to surface O_3 and SOA have been evaluated through chemical transport models (CTMs) at different spatial scales (Carlton and Baker, 2011;Fu and Liao, 2014;Jiang et al., 2019b;Zhang et al., 2020). Fu and Liao (2012) used the

70   Goddard Earth Observing System chemical transport model (GEOS-Chem) to quantitate the impact of biogenic emissions on O_3 in China over the year 2001-2006 and found that the difference in O_3 concentrations induced by interannual variability of BVOCs could be 2-5%. Based on the Weather Research and Forecasting model coupled with Chemistry (WRF-Chem), Situ et al. (2013) reported that about 57% higher O_3 formed from isoprene in urban areas than in rural areas in the PRD. In addition to the impact on surface O_3, Wu et al. (2020) studied the contributions of BVOCs to SOA in China in 2017 by using the

75   Community Multiscale Air Quality (CMAQ) and the result indicated that BVOCs are the main source of the formation of SOA in summer, which was up to 70%. Qin et al. (2018) investigated the biogenic SOA (BSOA) during summertime in 2012 and found that a high level of BSOA concentration appeared in Sichuan Basin. However, previous studies only focused on the impacts of BVOCs estimated by the specific LAI and LC satellite products on air quality. The uncertainties in BVOC estimations induced by different satellite products also have an impact on O_3 and SOA concentrations. Kim et al. (2014)

80   showed that the different PFTs distributions had a significant impact on hourly and local O_3, which was up to 13 ppb. Wang et al. (2020b) evaluated that the impacts on O_3 reached 20% by using different LC datasets in BVOC emissions in the YRD. The influence of these uncertainties on air quality was not well quantified and the bias in air quality remained unclear in China. Therefore, it is necessary to conduct a comprehensive analysis of the influence of different satellite products on BVOC emissions as well as the further impact on air quality.

85

In this study, the objectives are to estimate the difference in BVOC emissions induced by different LAI and LC databases in China and study the effects of differences in BVOC emissions on surface O_3 and SOA concentration in China. We used three LAI satellite datasets and three LC satellite datasets as the MEGANv2.1 inputs to estimate the BVOC emissions and then determined their impacts on air quality by using a source-oriented model. Section 2 introduces the MEGAN model, the source-

90   oriented CMAQ model, and datasets. The model performance, BVOC estimations based on different satellite products, as well as the impact of BVOCs on atmospheric pollutants are described in Section 3, while Section 4 concludes the study.

2 Methodology

2.1 Model setup

An updated source-oriented CTM was applied to determine O_3 and SOA concentrations from BVOCs based on the CMAQ

95   model v5.0.1 (Byun and Schere, 2006). The model utilizes a revised SAPRC-11 photochemical mechanism (S11) (Carter and Heo, 2013), which includes a more explicit description of isoprene oxidation chemistry to improve isoprene aerosol predictions

(Ying et al., 2015). Changes in the SOA module includes the surface uptake of dicarbonyls and isoprene epoxides, as well as predictions of glyoxal and methylglyoxal (Ying et al., 2015). The aerosol yields are updated to account for vapor wall loss during chamber experiments as described by Zhang et al. (2014). The S11 gas phase mechanism and the SOA module are further expanded with a precursor tracking scheme to track emissions from different sources separately so that the formation of SOA can be determined. The complete description of SOA source tracking has been described by Zhang and Ying (2011) and Wang et al. (2018b), and a brief introduction is described below.

The modified S11 mechanism expands the specific original reactions into two sets of similar reactions to track the formation of O_3 and SOA. The concentrations of O_3 from different VOC sources (henceforth $O_3\_VOC_i$) were determined by the source-oriented method (Ying and Krishnan, 2010). Based on the method, the non-reactive O_3 tracer is used to track O_3 attributed to BVOCs, which is tagged as $O_3\_VOC_{bio}$ and directly predicted. The descriptions of O_3 source apportionment see detailed in Wang et al. (2019). As for SOA, the specific source X (for instance, biogenic source) is tracked by adding a superscript X on the precursors related to SOA (like TERP, the abbreviation of monoterpene in the S11 photochemical mechanism) and their products, while the contributions from all other sources are simulated based on none-tagged TERP. The tagged specie $TERP^x$ reacts with OH to form the primary product $TRPRXN^x$, which is the counter species for aerosol precursor from monoterpenes and subsequently formed semi-volatile oxidation products SV_TRP1^x and SV_TRP2^x based on the two-product approach and thus determines the fine mode SOA species $ATRP1^x$ and $ATRP2^x$ due to gas-to-particle partitioning. By considering those species with the superscript X, it is possible to track the SOA formed by ATRP of source X. The contributions of other precursors of SOA are calculated using the same approach.

The WRF model v3.6.1 was used to generate meteorological conditions for MEGAN and CMAQ. The modeling domain in WRF was 36 km × 36 km in horizontal spatial resolution, which covers China and its surrounding countries in East Asia (Fig. S1) (Zhang et al., 2012). The boundary and initial conditions applied in WRF were from the National Centers for Environmental Prediction (NCEP) Final (FNL) Operational Model Global Tropospheric Analyses dataset (available at http://rda.ucar.edu/datasets/ds083.2/, last access: 18 May 2022). The model configurations are similar to the previous studies (Wang et al., 2018b;Wang et al., 2020a;Zhu et al., 2021) and Table S1 briefly lists the physical options used for the WRF model. The MEGANv2.1 was applied to estimate 19 compound classes of BVOCs (Guenther et al., 2012). In MEGAN, the LC and LAI datasets in 2016 were used and then were gridded to the same spatial resolution to generate PFTs fractions and LAIv maps as inputs for the model. The CMAQ model used the same horizontal resolution as WRF with a horizontal domain of 197 × 127 grid cells. This domain covers China and its surrounding areas (Fig. S1). The meteorological conditions as inputs to CMAQ model were provided by the WRF model v3.6.1. The anthropogenic emissions of China used the datasets from Multiresolution Emission Inventory for China (MEIC; available at http://www. meicmodel.org, last access:3 May 2022). Since the MEIC only provides anthropogenic emissions for China, anthropogenic emissions from foreign countries were provided by the Emissions Database for Global Atmospheric Research (EDGAR) v4.3 (available at http://edgar.jrc.ec.europa.eu/overview.php? v=_431,

last access: 10 May 2022). The MEIC inventory is widely used in air quality studies in China (Li et al., 2017b;Hu et al., 2016;Wu et al., 2020). It had an improvement in a vehicle emission inventory with high resolution (Zheng et al., 2014), and a non-methane VOC mapping approach for different chemical mechanisms (Li et al., 2014). The EDGAR is a grided emissions inventory with a high horizontal resolution of 0.1°×0.1° (Saikawa et al., 2017).

2.2 Data description

LAI and PFTs are key parameters for BVOC estimations. Three LC datasets were applied as PFTs inputs, including the Moderate Resolution Imaging Spectroradiometer (MODIS) MCD12Q1 LC products (Friedl and Sulla-Menashe, 2019), the Copernicus Climate Change Service (C3S) LC products (C3S, 2021), and the Copernicus Global Land Service (CGLS) LC products (Buchhorn et al., 2020). MCD12Q1 provides yearly global LC maps from 2001 to 2020 with spatial resolution at 500 m, which has been widely used in previous studies (Guenther et al., 2006;Wang et al., 2018a;Wu et al., 2020). Thus, MCD12Q1 is chosen as the baseline LC input for MEGANv2.1 to investigate the model performance with different LAI satellite products. Sources of these products are listed in Table S2. PFTs used in the MEGAN model adopt the scheme used for Community Land Model v4.0 (CLM4) (Guenther et al., 2012). Three LC maps are first re-gridded to the CMAQ domain (Fig. S2). Secondly, LC types are categorized into eight vegetation types according to legend descriptions of LC maps. Lastly, eight vegetation types are further reclassified into CLM-15 PFTs based on the climate rules described in Bonan et al. (2002). Figure 1 shows the simulation domain with the spatial distribution of major PFTs. The three datasets show a consistent distribution of grass in northwest China, but they display distinct PFTs in central and southern China. Cropland is the dominant PFT in central and southern China in the C3S LC map. Although MCD12Q1 and CGLS LC both show a large area in central and southern China, the area fraction of the broadleaf tree in CGLS LC is higher than that in MCD12Q1 (Fig. 1 and Fig. S3).

The Global LAnd Surface Satellite (GLASS) (Xiao et al., 2014;Xiao et al., 2016), the MODIS MOD15A2H version 6 (MOD15) (Myneni et al., 2015), and the CGLS LAI products (Fuster et al., 2020) were applied as LAI inputs for MEGANv2.1. The spatial resolutions of GLASS, MOD15, and CGLS are 500m, 500m and 300m, respectively, while the temporal resolutions of these three products are 8 days, 8 days, and 10 days, respectively. Sources of these products are listed in Table S2. According to validation results in Xiao et al. (2016), GLASS shows better consistency than MOD15 in high resolution in LAI maps, while CGLS is slightly less accurate than MOD15 (Fuster et al., 2020). Therefore, the GLASS is used as the baseline LAI input. In the MEGAN model, the grid average LAI is divided by the fraction of the grid that is covered by vegetation to represent the LAI of vegetation covered surface, which is referred to LAIv (Guenther et al., 2006). Figure 2 represents the spatial distribution of LAI from three satellite datasets in the summer of 2016. The MOD15 LAI dataset used in C2 shows differences from C1, especially in south China, where the GLASS LAIv is about 50% higher than the MOD15 LAIv. The MOD15 LAIv is lower in NCP than other products because the MOD15 underestimates the LAI of maize and wheat in NCP (Yang et al., 2015;Wang et al., 2022).

Table 1 presents the setup of the simulation scenarios. Scenarios C1 to C3 use MCD12Q1 as the PFTs input and different LAI inputs to investigate the effects of varied LAI datasets on BVOC emissions, while the impacts of different PFTs maps on BVOC estimations are studied in scenarios C1, C4, and C5, which use the GLASS as the LAI input. It should be noted that those experiments use the same meteorological conditions provided by the WRF model for BVOC estimations. Besides BVOC simulations, a one-year CMAQ simulation with five different sets of MEGAN input data is conducted in the year 2016 in China with the same meteorological conditions and anthropogenic emissions to investigate the impacts of BVOCs on O_3 and SOA concentrations. It is worth noting that the meteorological conditions remain constant when simulating and the model chemistry does not affect them.

3 Results and discussion

3.1 Model performance

Temperature (T2), relative humidity (RH), wind speed (WS) and wind direction (WD) at 10 m above the surface were compared to observations from the National Climate Data Center (NCDC, available at https://www.ncei.noaa.gov/access, last access: 13 May 2022). The statistical measures and results are shown in Table S3 and Table S4, respectively. The T2 predictions for the entire year show a negative mean bias (MB) value, which is slightly lower than the benchmarks suggested by Emery et al. (2001). This is primarily due to the overestimation of cloud coverage in the WRF model, resulting in an underestimated T2 (Wu et al., 2020). Although biases exist in the T2 simulation, the yearly long WRF simulation in this study shows relatively small biases compared to previous studies (Wu et al., 2020;Wang et al., 2018a), and the daily variation of temperature is successfully simulated for most cities in China (Fig. S4). The gross error (GE) values of WS are within the acceptable criteria of 2 for all seasons, but the WRF model still overpredicts the WS. The MB values of WD meet the benchmarks of ±10 in all seasons, indicating good agreement between model predictions and observations. However, the GE values exceed the benchmarks of ±30. Moreover, the predicted RH in spring and winter shows a slight underestimation compared to observations, whereas in summer and fall, it is overestimated. Generally, the performance of the WRF model in this study is comparable to previous studies (Hu et al., 2016;Wang et al., 2018a;Wang et al., 2010;Ma et al., 2021). Therefore, the meteorological conditions predicted by the WRF model are acceptable inputs for the CMAQ model in follow-up research.

Hourly observations from the publishing website of the China National Environmental Monitoring Center (available at http://www.cnemc.cn/, last access: 4 May 2022) were used to validate the CMAQ model prediction of O_3 and $PM_{2.5}$. In order to investigate the impacts of varied total BVOC emissions on air pollutants, the model performance was evaluated separately for different cases. Table S5 presents the model performance statistics for maximum daily averaged 1h (MDA1) O_3 and maximum daily averaged 8h (MDA8) O_3 in 2016, including mean observations (OBS), mean predictions (PRE), mean fractional bias (MFB), mean fractional error (MFE), mean normalized bias (MNB), and mean normalized error (MNE). Cut-off concentrations of 60 ppb were used for MDA1 O_3 and MDA8 O_3 in this validation, which was suggested by the US EPA

(EPA, 2005). In general, the model performance of MDA1 O_3 and MDA8 O_3 in China, including its important regions, meets the model performance benchmarks suggested by EPA (2005). The MNB values of MDA1 O_3 in China range from 0.02~0.05, which fall within the criteria of ±0.15. Similarly, the MNE values of MDA1 O_3 range from 0.18~0.19, which fall within the criteria of ±0.3. Notable, the MDA1 O_3 concentration in the PRD shows better consistency with observations than in the YRD and NCP. Moreover, the statistical values of MDA1 O_3 in C4 are closer to benchmarks, indicating the better performance of the model simulation in C4. While the MNB values of MDA8 O_3 are slightly higher than those of MDA1 O_3, they still meet the criteria.

Table S6 presents the model performance statistics on $PM_{2.5}$. The statistical values of $PM_{2.5}$ in all cases are within the criteria (MFB ≤ ±60 % and MFE ≤ 75 %) suggested by Boylan and Russell (2006). However, the predicted $PM_{2.5}$ is slightly lower than observations, as the negative MFB values indicate. The MNB values in the YRD are slightly higher compared to other regions, while MFE and MNE values are higher in the PRD. In comparison with other cases, the statistical values of $PM_{2.5}$ in C4 are lower, indicating a better performance of $PM_{2.5}$ in C4. Therefore, the BVOC emissions in C4 generated by C3S LC and GLASS are the best BVOC inventory in this study. While different accuracies of LAI satellite products were used for C1, C2, and C3, similar statistics values indicate that the accuracies of these products have no significant impact on the model performance. Additionally, the overall statistical values meet the criteria in all cases, indicating that the O_3 and $PM_{2.5}$ are well captured by the model. Generally, the simulation results of air pollutants in this study are acceptable for the source apportionment study of O_3 and SOA and are comparable to other studies (Hu et al., 2016;Wu et al., 2020;Liu et al., 2020).

3.2 Simulated BVOC emissions in China

3.2.1 Quantity of BVOC emissions

Table 2 shows the total amount of BVOC emissions and its major components of each case in China in 2016. The use of different LAI and LC datasets as the MEGAN inputs has an impact on BVOC emissions. Isoprene constitutes the largest share of BVOC emissions, accounting for an average of 54%. The variation in the isoprene emission is the primary reason for the discrepancy in total BVOC emissions between each case. Among all cases, C5 exhibits the highest BVOC emissions of 37.39 Tg, with the isoprene emission at 22.73 Tg, also the highest. In contrast, BVOC emissions of 25.42 Tg and the isoprene emission of 12.1 Tg in C4 are the lowest. The difference between C1, C2 and C3 indicates the impact of LAI on BVOC emissions. In addition to the impact of LAI datasets, the LC dataset used in C4 leads to a 21.4% decrease in isoprene emissions compared to C1. Moreover, C5, which uses the CGLS LC dataset, shows an 8% increase in the isoprene emission than C1 due to a higher percentage of broadleaf tree cover (Fig. S3 and Fig. S5). Although C5 has 1.29 Tg higher BVOC emissions than C1, emissions of monoterpenes, sesquiterpenes, and other VOCs are lower than those in C1. This can be attributed to the difference in the distribution of needleleaf trees and shrubs between C1 and C5, which is consistent with the findings of Wang et al. (2018a) (Fig. S3 and Fig. S5).

3.2.2 Temporal and spatial variation of BVOC emissions

Figure 3 illustrates the seasonal variations of isoprene, monoterpenes, sesquiterpenes, and total BVOC emissions in China. It is noteworthy that the use of different LAI and LC products has a significant impact on the temporal variability of BVOC emissions. Despite this, the seasonal patterns of BVOC emissions remain relatively consistent across all cases, with peak emissions occurring predominantly during summer, accounting for 60.9% to 63.8% of the total BVOC emissions, compared to only 2.9% to 3.4% in winter. Besides, the differences in BVOC emissions between C1 and the other cases are more pronounced during the summer months, as BVOC emissions are highly sensitive to changes in temperature and radiation in the atmosphere (Guenther et al., 2006;Guenther et al., 2012). Isoprene is the largest contributor to BVOCs, with summer emissions ranging from 7.94 to 14.79 Tg. The percentage of winter monoterpenes in the total monoterpenes is higher than that of isoprene and sesquiterpenes, probably because isoprene and sesquiterpenes are more sensitive to temperature changes than monoterpenes (Ibrahim et al., 2010;Bai et al., 2015). C4 shows the lowest total BVOC emissions along with its primary species during each season. Although C5 has the highest isoprene emission compared to the other cases, its monoterpene and sesquiterpene emissions are lower than those in C1 and C3. This can be because CGLS LC has a higher distribution of broadleaf trees with a high isoprene EF and a lower distribution of grass with high monoterpene and sesquiterpene EF compared to those in MCD12Q1 (Fig. S3).

Since a large proportion of BVOCs are released in summer, contributing about 62% of total annual emissions, the analysis of the spatial distribution is mainly concentrated on summer BVOC emissions. Figure 4 illustrates the spatial distribution of total BVOCs, isoprene, monoterpenes, and sesquiterpenes during summer in C1 as well as the comparisons between C1 and the other cases. In general, the difference in the spatial distribution of BVOCs mainly focuses on central and southeastern China, and the differences induced by different LC products are more significant than by different LAI products. Isoprene, monoterpenes, and sesquiterpenes emissions show similar distribution patterns with hotspots primarily located in central and southeastern China, as shown in Fig. 4 (panels f, k and p). This is due to the high density of tree covers in those regions. Although the GLASS has the same temporal resolution of 8 days as MOD15, differences between the two products still play an important role in impacting the BVOC emissions (Fig. 2 and Fig. 4b). According to Fig. 4 (panels a and q), the emission distribution of isoprene and sesquiterpene differs between C1 and C2, consistent with the difference in GLASS and MOD15 in summer (Fig. 2). Compared to C2 and C3, the changes in the spatial distribution of BVOC emissions in C4 and C5 are more significant. This is because the impact on BVOC emissions decreases when LAIv exceeds 3 (Guenther et al., 2012). Higher BVOC emissions in southern China in C1 compared to C4 are due to higher vegetation cover in C1, as shown in Fig. 4 (panels i, n and s). C4 uses the C3S LC as the model input, with crops dominating nearly half of China. This results in lower BVOC estimations in C4, as the relatively low EF of the crop for BVOC emissions compared to the other PFTs (Fig. 1 and Fig. S5). The spatial distribution of isoprene emission in C5 is conspicuously different from that in C1, which is consistent with a difference in the broadleaf tree distribution (Fig. S5). Although C5 shows a higher forest cover than C1 in the north of China,

the isoprene emission in C1 is higher than in C5 likely due to the difference in the grass distribution and the impact of temperature. Cooler temperatures at higher latitudes inhibit the release of isoprene from forests (Guenther et al., 2006).

3.2.3 Comparison with previous studies

Table 3 illustrates the annual BVOC emissions estimated by MEGAN in China in this study and previous studies. The annual BVOC emissions in this study range from 25.42 ~ 37.39 Tg, within the range of 17.30 ~ 54.60 Tg reported in the literature from 2001 to 2018. BVOC emissions estimated by this study are higher than 18.85 and 23.54 Tg estimated by Fu and Liao (2012), and Wu et al. (2020), respectively. However, the results of this study are lower than 58.9 Tg estimated by Li et al. (2020) for 2018. Several factors may account for the differences between this study and previous studies. One major reason could be the increase in forest coverage. According to National Forest Resources Census reports, forest coverage increased by about 18.8% between 2003 and 2013 (FGA, 2006, 2014). In addition, BVOC emissions can be influenced by the inputs and algorithms used in the MEGAN model. In this study, the default EFs listed in Guenther et al. (2012) are used for all BVOC species. Fu and Liao (2012) used a set of EFs with 25 PFTs for isoprene and monoterpenes, which generally have lower EFs than the default ones used in MEGAN. Consequently, their study reported much lower BVOC emissions of 18.85 Tg compared to our findings. Wu et al. (2020) used the same datasets of MODIS MOD15A2H and MODIS MCD12Q1 as this study but estimated lower BVOC emissions due to lower area fractions of high isoprene-emitting broadleaf trees (Guenther et al., 2012) and no inclusion of crop area in calculations for China. Moreover, Li et al. (2020) reported a considerable difference in BVOC emissions compared to this study, mainly due to the combined effect of emission rate and PFTs. Liu et al. (2020) produced the basal emission rates for 192 plant species and categorized them into 82 PFTs for China, resulting in more BVOC estimates. Besides, the higher estimate of 35.48 Tg for 2016 by Wang et al. (2021) may be attributed to the overestimated temperature. This is the primary reason for the significant difference between this study and theirs. In conclusion, uncertainties in the MEGAN simulations can be attributed to these factors in different years, and such uncertainties can lead to significant differences between this study and previous studies. Nonetheless, this study suggests that the simulated BVOC emissions fall within acceptable limits compared to the previous studies.

3.3 Sensitivity of O_3 to BVOC emissions

3.3.1 Spatial distribution of O_3

Figure 5 displays the spatial distribution of MDA1 O_3 and MDA8 O_3 concentrations formed by the BVOCs during the summer in C1 as well as the difference between C1 and other cases. Changing the LC dataset in the MEGAN model has a more significant impact on O_3 concentrations compared to changing the LAI dataset. The O_3 concentration hotspots are mainly concentrated in central and eastern China, with MDA1 O_3 concentrations exceeding 12 ppb in C1. This is possibly due to the combined effect of BVOC emissions and the Asian summer monsoon. The monsoon carries oceanic air masses with low O_3 concentrations and transports O_3 from southern to central and northern China (Zhao et al., 2010;Li et al., 2018). In Fig. 5d, the

spatial distribution of O_3 concentration in C4 differs from that of C1, especially in central and eastern China, where the relative difference exceeds 52%. Although C5 has higher BVOC emissions than C1 in southern China, it has little impact on O_3 formation (Fig. 4). This may be due to the effect of O_3-NO_x-VOC sensitivity, as reported by Jin and Holloway (2015). These regions belong to NO_x-limited regions, in which NO_x is limited, but VOCs are abundant. Thus, the higher BVOC emissions have minimal effects on the O_3 formation. Conversely, areas with low VOC emissions, such as the NCP and YRD, will contribute more to the O_3 formation when VOC emissions increase. The spatial distribution pattern of MDA8 O_3 is similar to that of MDA1 O_3 in C1, but its concentration is 3-6 ppb lower than that of MDA1 O_3.

3.3.2 Temporal distribution of O_3

Figure 6 illustrates the contribution of BVOC emissions to MDA1 O_3 and MDA8 O_3 in China and important regions in different seasons. O_3 concentrations, which is formed by BVOCs, show seasonal variations in China, with the highest in summer and the lowest in winter. This is a result of the interplay between BVOC emissions and wind. In the PRD, wind plays an important role in O_3 concentrations (Fig. S6), as it can transport clean oceanic air masses to the southeast of China, decreasing local O_3 concentrations (Zhao et al., 2010). However, wind transports heavy pollutants from northern to southern China in the fall, increasing O_3 concentrations in the PRD (Li et al., 2018). In addition, compared to other regions, the temperature variation in the PRD is not significant (Table S7). Therefore, the seasonal variations of O_3 are not significant in the PRD due to the combined effect of wind and temperature. The seasonal variation of O_3 formed by BVOCs also varies in different cases. In China, MDA1 O_3 concentrations increase by approximately 40-50% in summer compared to spring, whereas C2 increases by 75%. C2 also shows the highest increase in O_3 concentrations in important regions from spring to summer. Moreover, in the YRD, MDA1 O_3 in C1 is 78% higher than in C4 because of the O_3-NO_x-VOC sensitivity, with higher BVOC emissions in VOC-limited areas leading to higher O_3 formation (Jin and Holloway, 2015). In China and other important regions, MDA8 O_3 shows a temporal distribution similar to MDA1 O_3 in all cases. However, the contribution of MDA8 O_3 to the fall season is lower than its contribution to the spring season, which contrasts with MDA1 O_3.

3.4 Sensitivity of SOA to BVOC emissions

3.4.1 Spatial distribution of SOA and components

Figure 7 presents the spatial distribution of BSOA during summer in C1 and the difference between C1 and other cases. Changing the LC dataset in the MEGAN model has a more significant impact on BSOA formation than changing the LAI dataset. The hotspots of BSOA are mainly concentrated in central and eastern China, with Sichuan Basin (Fig. S1) having the highest BSOA concentration of up to 9.8 μg m^{-3}. This is because high surface winds transport BSOA from southern China to central China, where low wind speeds and the topography of the Sichuan Basin hinder pollutant diffusion, leading to BSOA accumulation (Li et al., 2017a). The difference in BSOA concentrations between C1 and C2 is minor due to the slight change in BVOCs. In contrast, the difference in BSOA concentrations between C1 and C4 is significant due to the use of different LC

datasets. As shown in Fig. 7d, the difference in BSOA concentrations between C1 and C4 is noticeable, especially in central and eastern China, where the relative difference is over 140% in summer. The differences in the spatial distribution of BSOA between C1 and C5 are similar to those in isoprene, suggesting that BSOA concentrations are more sensitive to isoprene emissions. Considering the share of BSOA in the total SOA concentration in summer, the difference in BVOC emissions due to changing the MEGAN inputs can significantly impact SOA concentrations estimated by CMAQ.

Figure 8 displays the spatial distribution of SOA formed by isoprene (ISOA), monoterpenes (MSOA) and sesquiterpenes (SSOA) during summer in C1 as well as the difference between C1 and the other cases. The ISOA, MSOA and SSOA show a similar spatial distribution in China. According to Fig. 8 (panels a, b and c), high SOA concentrations from these three BVOC species are mainly concentrated in central and eastern China. This phenomenon is likely due to the combined effect of BVOC emissions and meteorological conditions in these areas. A large amount of SOA is generated in southern China and then transported to central and eastern China due to wind effects in summer. The ISOA is the most crucial contributor to BSOA, which is one time higher than MSOA and 1.5 times higher than SSOA. Comparing C1 with other cases, the difference in ISOA concentrations basically shows a certain correlation with the difference in BVOCs (Fig. 4). The relative difference in ISOA concentrations between C1 and C4 can reach 160% in eastern China, which is higher than that in MSOA and SSOA. This can be attributed to the large discrepancy in their isoprene emission (Fig.8j, k, and l). ISOA concentrations in southeastern China are lower in C1 than in C5, but MSOA and SSOA concentrations are higher than in C5, which is due to the difference in BVOC estimations. Changing the MEGAN inputs has a large impact on isoprene emissions, which are the main contributor to BVOC emissions. This further impact the formation of SOA.

3.4.2 Temporal distribution of SOA

Figure 9 illustrates the seasonal variation in BSOA concentrations in China and the important regions for all cases. In general, the differences in BSOA concentrations between each case are more significant in summer than in other seasons. The BSOA concentration follows the seasonal cycle of summer > spring > fall > winter in China, NCP, and YRD. However, the higher BSOA concentration in the PRD occurs during spring, and this can be attributed to changes in wind direction, from erratic winds in spring to southerly winds in summer, as shown in Fig. S7. BSOA concentrations vary slightly between C1, C3, and C5 in China, but the differences are significant between C2 and C4, particularly in the YRD, where the summer BSOA in C1 is 2.5 times higher than in C4. This is because the summer BVOC emissions in C1 are higher than those in C4 in the YRD (Fig. S8) and thus formed more BSOA. C1 tends to have higher BSOA concentrations than C5 in most regions of China. However, this differs in the PRD, where C5 has higher BSOA concentrations due to higher isoprene emissions (Fig. 4).

4 Conclusion

In this study, we used the different LAI and LC datasets as the MEGAN inputs to estimate the BVOC emissions in 2016 over China and then utilized the WRF-CMAQ model to quantify the contribution of BVOCs to O_3 and SOA concentrations. Besides, the impact induced by those inputs on O_3 and SOA formation was also evaluated. Five experiments were conducted based on three LAI satellite products (GLASS, MOD15, and CGLS) and three LC satellite products (MCD12Q1, C3S, and CGLS). According to model validations, C4 with GLASS and C3S LC was the better choice for China BVOC estimations than other scenarios. BVOC emissions in China ranged from 25.42 to 37.39 Tg in 2016 and were mainly concentrated in central and southeastern China due to the high density of tree covers in those regions. In comparison with LAI inputs, using different LC satellite products had a more significant impact on BVOC emissions.

The O_3 formed by BVOCs was mainly concentrated in central and eastern China, where O_3 concentrations could reach 12 ppb. This was likely due to the combined effect of BVOC emissions and the summer monsoon. According to the sensitivity analysis, C1 contributed the most to the summer O_3, which was 78% higher than C4 in the YRD. The BSOA was also concentrated in central and eastern China, especially in Sichuan Basin, where the BSOA concentration was up to 9.8 $\mu g\ m^{-3}$. The differences in BSOA concentrations between C1 and C2 are inconspicuous due to the slightly change in BVOCs induced by LAI inputs. In contrast, the LC inputs show higher impacts on BSOA concentrations. This is the same as O_3. Therefore, changing LAI and LC datasets in the model impacts O_3 and SOA formation, where the LC shows a more pronounced effect than LAI. Our results suggest that the uncertainties in MEGAN inputs should be carefully considered in future O_3 and SOA simulations.

From 2000 to 2017, the global leaf area of vegetation increased by 6.6% due to direct land-use management, which may also enhance BVOC emissions and further affect air quality. Thus, the findings of this study can be extended to other regions and global scales, suggesting an urgent need to construct a reliable BVOC emission inventory for local and global scales and evaluate their impacts on air quality. However, the limitation in observed data of BVOCs and organic components impedes the construction of an accurate emission inventory. Therefore, field measurements are needed to provide more data for model validations. In addition, urban BVOC emissions play important roles in urban air quality. It would be interesting to study the impact of biogenic sources on urban air quality using high-resolution LC satellite maps.

Author contributions. JM conducted the modelling and write the paper. SZ and SW assisted with data analysis. PW and HZ designed the study, discussed the results, and edited the paper.

Competing interests. The authors declare that they have no conflict of interest.

Financial support. The DFG-NSFC Sino-German AirChanges project (448720203), National Natural Science Foundation of China (42077194/42061134008), and Shanghai International Science and Technology Partnership Project (No. 21230780200) funded this work.

References

Bai, J., Guenther, A., Turnipseed, A., and Duhl, T.: Seasonal and interannual variations in whole-ecosystem isoprene and monoterpene emissions from a temperate mixed forest in Northern China, Atmospheric Pollution Research, 6, 696-707, https://doi.org/10.5094/APR.2015.078, 2015.

Boylan, J. W., and Russell, A. G.: PM and light extinction model performance metrics, goals, and criteria for three-dimensional air quality models, Atmos. Environ., 40, 4946-4959, https://doi.org/10.1016/j.atmosenv.2005.09.087, 2006.

Buchhorn, M., Smets, B., Bertels, L., DeRoo, B., Lesiv, M., Tsendbazar, N.-E., Herold, M., and Fritz, S.: Copernicus Global Land Service: Land Cover 100m: collection 3: epoch 2019: Globe (V3.0.1) [Data set], Zenodo, https://doi.org/10.5281/zenodo.3939050, 2020.

Byun, D., and Schere, K. L.: Review of the Governing Equations, Computational Algorithms, and Other Components of the Models-3 Community Multiscale Air Quality (CMAQ) Modeling System, Appl. Mech. Rev., 59, 51-77, 10.1115/1.2128636, 2006.

C3S: Product User Guide and Specification, 2021.

Calfapietra, C., Fares, S., Manes, F., Morani, A., Sgrigna, G., and Loreto, F.: Role of Biogenic Volatile Organic Compounds (BVOC) emitted by urban trees on ozone concentration in cities: A review, Environ. Pollut., 183, 71-80, 10.1016/j.envpol.2013.03.012, 2013.

Carlton, A. G., and Baker, K. R.: Photochemical Modeling of the Ozark Isoprene Volcano: MEGAN, BEIS, and Their Impacts on Air Quality Predictions, Environ. Sci. Technol., 45, 4438-4445, 10.1021/es200050x, 2011.

Carter, W. P. L., and Heo, G.: Development of revised SAPRC aromatics mechanisms, Atmos. Environ., 77, 404-414, https://doi.org/10.1016/j.atmosenv.2013.05.021, 2013.

Emery, C., Tai, E., and Yarwood, G.: Enhanced meteorological modeling and performance evaluation for two texas episodes, Report to the Texas Natural Resources Conservation Commission, prepared by ENVIRON, International Corp., Novato, CA, 2001.

Emmerson, K. M., Cope, M. E., Galbally, I. E., Lee, S., and Nelson, P. F.: Isoprene and monoterpene emissions in south-east Australia: comparison of a multi-layer canopy model with MEGAN and with atmospheric observations, Atmos. Chem. Phys., 18, 7539-7556, 10.5194/acp-18-7539-2018, 2018.

EPA, U. S.: Guidance on the Use of Models and Other Analyses in Attainment Demonstrations for the 8-hour Ozone NAAQS, EPA-454/R-05-002, 2005.

Fehsenfeld, F., Calvert, J., Fall, R., Goldan, P., Guenther, A. B., Hewitt, C. N., Lamb, B., Liu, S., Trainer, M., Westberg, H., and Zimmerman, P.: Emissions of volatile organic compounds from vegetation and the implications for atmospheric chemistry, Global Biogeochem Cycles., 6, 389-430, https://doi.org/10.1029/92GB02125, 1992.

The Sixth National Forest Resources Inventory: http://www.forestry.gov.cn/portal/main/s/65/content-90.html, 2006.

FGA, C.: The Eighth National Forest Resources Inventory, 2014.

Friedl, M., and Sulla-Menashe, D.: MCD12Q1 MODIS/Terra+Aqua Land Cover Type Yearly L3 Global 500m SIN Grid V006 [Data set], NASA EOSDIS Land Processes DAAC, https://doi.org/10.5067/MODIS/MCD12Q1.006, 2019.

Fu, Y., and Liao, H.: Simulation of the interannual variations of biogenic emissions of volatile organic compounds in China: Impacts on tropospheric ozone and secondary organic aerosol, Atmos. Environ., 59, 170-185, https://doi.org/10.1016/j.atmosenv.2012.05.053, 2012.

Fu, Y., and Liao, H.: Impacts of land use and land cover changes on biogenic emissions of volatile organic compounds in China from the late 1980s to the mid-2000s: implications for tropospheric ozone and secondary organic aerosol, Tellus B., 66, 10.3402/tellusb.v66.24987, 2014.

Fuster, B., Sánchez-Zapero, J., Camacho, F., García-Santos, V., Verger, A., Lacaze, R., Weiss, M., Baret, F., and Smets, B.: Quality Assessment of PROBA-V LAI, fAPAR and fCOVER Collection 300 m Products of Copernicus Global Land Service, Remote Sens., 12, 10.3390/rs12061017, 2020.

Guenther, A., Hewitt, C. N., Erickson, D., Fall, R., Geron, C., Graedel, T., Harley, P., Klinger, L., Lerdau, M., McKay, W. A., Pierce, T., Scholes, B., Steinbrecher, R., Tallamraju, R., Taylor, J., and Zimmerman, P.: A global model of natural volatile organic compound emissions, J. Geophys. Res. Atmos., 100, 8873-8892, https://doi.org/10.1029/94JD02950, 1995.

Guenther, A., Karl, T., Harley, P., Wiedinmyer, C., Palmer, P. I., and Geron, C.: Estimates of global terrestrial isoprene emissions using MEGAN (Model of Emissions of Gases and Aerosols from Nature), Atmos. Chem. Phys., 6, 3181-3210, 10.5194/acp-6-3181-2006, 2006.

Guenther, A. B., Jiang, X., Heald, C. L., Sakulyanontvittaya, T., Duhl, T., Emmons, L. K., and Wang, X.: The Model of Emissions of Gases and Aerosols from Nature version 2.1 (MEGAN2.1): an extended and updated framework for modeling biogenic emissions, Geosci. Model Dev., 5, 1471-1492, 10.5194/gmd-5-1471-2012, 2012.

Hu, J., Chen, J., Ying, Q., and Zhang, H.: One-year simulation of ozone and particulate matter in China using WRF/CMAQ modeling system, Atmos. Chem. Phys., 16, 10333-10350, 10.5194/acp-16-10333-2016, 2016.

Ibrahim, M. A., Maenpaa, M., Hassinen, V., Kontunen-Soppela, S., Malec, L., Rousi, M., Pietikainen, L., Tervahauta, A., Karenlampi, S., Holopainen, J. K., and Oksanen, E. J.: Elevation of night-time temperature increases terpenoid emissions from Betula pendula and Populus tremula, J Exp Bot, 61, 1583-1595, 10.1093/jxb/erq034, 2010.

Jiang, J., Aksoyoglu, S., Ciarelli, G., Oikonomakis, E., El-Haddad, I., Canonaco, F., O'Dowd, C., Ovadnevaite, J., Cruz Minguillon, M., Baltensperger, U., and Prevot, A. S. H.: Effects of two different biogenic emission models on modelled ozone and aerosol concentrations in Europe, Atmos. Chem. Phys., 19, 3747-3768, 10.5194/acp-19-3747-2019, 2019a.

Jiang, J. H., Aksoyoglu, S., Ciarelli, G., Oikonomakis, E., El-Haddad, I., Canonaco, F., O'Dowd, C., Ovadnevaite, J., Minguillon, M. C., Baltensperger, U., and Prevot, A. S. H.: Effects of two different biogenic emission models on modelled ozone and aerosol concentrations in Europe, Atmos. Chem. Phys., 19, 3747-3768, 10.5194/acp-19-3747-2019, 2019b.

Jin, X., and Holloway, T.: Spatial and temporal variability of ozone sensitivity over China observed from the Ozone Monitoring Instrument, J. Geophys. Res. Atmos., 120, 7229-7246, https://doi.org/10.1002/2015JD023250, 2015.

Kim, H. K., Woo, J. H., Park, R. S., Song, C. H., Kim, J. H., Ban, S. J., and Park, J. H.: Impacts of different plant functional types on ambient ozone predictions in the Seoul Metropolitan Areas (SMAs), Korea, Atmos. Chem. Phys., 14, 7461-7484, 10.5194/acp-14-7461-2014, 2014.

Laothawornkitkul, J., Taylor, J. E., Paul, N. D., and Hewitt, C. N.: Biogenic Volatile Organic Compounds in the Earth System, New Phytol., 183, 27-51, 2009.

Leung, D. Y. C., Wong, P., Cheung, B. K. H., and Guenther, A.: Improved land cover and emission factors for modeling biogenic volatile organic compounds emissions from Hong Kong, Atmos. Environ., 44, 1456-1468, 10.1016/j.atmosenv.2010.01.012, 2010.

Li, J., Zhang, M., Wu, F., Sun, Y., and Tang, G.: Assessment of the impacts of aromatic VOC emissions and yields of SOA on SOA concentrations with the air quality model RAMS-CMAQ, Atmos. Environ., 158, 105-115, https://doi.org/10.1016/j.atmosenv.2017.03.035, 2017a.

Li, L., Yang, W., Xie, S., and Wu, Y.: Estimations and uncertainty of biogenic volatile organic compound emission inventory in China for 2008–2018, Sci. Total. Environ., 733, 139301, https://doi.org/10.1016/j.scitotenv.2020.139301, 2020.

Li, L. Y., Chen, Y., and Xie, S. D.: Spatio-temporal variation of biogenic volatile organic compounds emissions in China, Environ. Pollut., 182, 157-168, https://doi.org/10.1016/j.envpol.2013.06.042, 2013.

Li, M., Zhang, Q., Streets, D. G., He, K. B., Cheng, Y. F., Emmons, L. K., Huo, H., Kang, S. C., Lu, Z., Shao, M., Su, H., Yu, X., and Zhang, Y.: Mapping Asian anthropogenic emissions of non-methane volatile organic compounds to multiple chemical mechanisms, Atmos. Chem. Phys., 14, 5617-5638, 10.5194/acp-14-5617-2014, 2014.

Li, M., Liu, H., Geng, G., Hong, C., Liu, F., Song, Y., Tong, D., Zheng, B., Cui, H., Man, H., Zhang, Q., and He, K.: Anthropogenic emission inventories in China: a review, National Science Review, 4, 834-866, 10.1093/nsr/nwx150, 2017b.

Li, S., Wang, T., Huang, X., Pu, X., Li, M., Chen, P., Yang, X.-Q., and Wang, M.: Impact of East Asian Summer Monsoon on Surface Ozone Pattern in China, J. Geophys. Res. Atmos., 123, 1401-1411, https://doi.org/10.1002/2017JD027190, 2018.

Liu, J., Shen, J., Cheng, Z., Wang, P., Ying, Q., Zhao, Q., Zhang, Y., Zhao, Y., and Fu, Q.: Source apportionment and regional transport of anthropogenic secondary organic aerosol during winter pollution periods in the Yangtze River Delta, China, Sci. Total. Environ., 710, 135620, https://doi.org/10.1016/j.scitotenv.2019.135620, 2020.

Ma, J., Shen, J., Wang, P., Zhu, S., Wang, Y., Wang, P., Wang, G., Chen, J., and Zhang, H.: Modeled changes in source contributions of particulate matter during the COVID-19 pandemic in the Yangtze River Delta, China, Atmos. Chem. Phys., 21, 7343-7355, 10.5194/acp-21-7343-2021, 2021.

Messina, P., Lathière, J., Sindelarova, K., Vuichard, N., Granier, C., Ghattas, J., Cozic, A., and Hauglustaine, D. A.: Global biogenic volatile organic compound emissions in the ORCHIDEE and MEGAN models and sensitivity to key parameters, Atmos. Chem. Phys., 16, 14169-14202, 10.5194/acp-16-14169-2016, 2016.

Myneni, R. B., Knyazikhin, Y., and Park, T.: MOD15A2H MODIS/Terra Leaf Area Index/FPAR 8-Day L4 Global 500m SIN Grid V006 [Data set], NASA EOSDIS Land Processes DAAC, https://doi.org/10.5067/MODIS/MOD15A2H.006, 2015.

NFGA: China Forest Resources Report (2014-2018), 1 ed., China Forestry Press, 2019.

Opacka, B., Muller, J.-F., Stavrakou, T., Bauwens, M., Sindelarova, K., Markova, J., and Guenther, A. B.: Global and regional impacts of land cover changes on isoprene emissions derived from spaceborne data and the MEGAN model, Atmos. Chem. Phys., 21, 8413-8436, 10.5194/acp-21-8413-2021, 2021.

Pfister, G. G., Emmons, L. K., Hess, P. G., Lamarque, J. F., Orlando, J. J., Walters, S., Guenther, A., Palmer, P. I., and Lawrence, P. J.: Contribution of isoprene to chemical budgets: A model tracer study with the NCAR CTM MOZART-4, J. Geophys. Res. Atmos., 113, https://doi.org/10.1029/2007JD008948, 2008.

Qin, M., Wang, X., Hu, Y., Ding, X., Song, Y., Li, M., Vasilakos, P., Nenes, A., and Russell, A. G.: Simulating Biogenic Secondary Organic Aerosol During Summertime in China, J. Geophys. Res. Atmos., 123, 11,100-111,119, https://doi.org/10.1029/2018JD029185, 2018.

Saikawa, E., Kim, H., Zhong, M., Avramov, A., Zhao, Y., Janssens-Maenhout, G., Kurokawa, J. I., Klimont, Z., Wagner, F., Naik, V., Horowitz, L. W., and Zhang, Q.: Comparison of emissions inventories of anthropogenic air pollutants and greenhouse gases in China, Atmos. Chem. Phys., 17, 6393-6421, 10.5194/acp-17-6393-2017, 2017.

Sindelarova, K., Granier, C., Bouarar, I., Guenther, A., Tilmes, S., Stavrakou, T., Muller, J. F., Kuhn, U., Stefani, P., and Knorr, W.: Global data set of biogenic VOC emissions calculated by the MEGAN model over the last 30 years, Atmos. Chem. Phys., 14, 9317-9341, 10.5194/acp-14-9317-2014, 2014.

Situ, S., Guenther, A., Wang, X., Jiang, X., Turnipseed, A., Wu, Z., Bai, J., and Wang, X.: Impacts of seasonal and regional variability in biogenic VOC emissions on surface ozone in the Pearl River delta region, China, Atmos. Chem. Phys., 13, 11803-11817, 10.5194/acp-13-11803-2013, 2013.

Situ, S., Wang, X., Guenther, A., Zhang, Y., Wang, X., Huang, M., Fan, Q., and Xiong, Z.: Uncertainties of isoprene emissions in the MEGAN model estimated for a coniferous and broad-leaved mixed forest in Southern China, Atmos. Environ., 98, 105-110, https://doi.org/10.1016/j.atmosenv.2014.08.023, 2014.

495 Stavrakou, T., Müller, J. F., Bauwens, M., De Smedt, I., Van Roozendael, M., Guenther, A., Wild, M., and Xia, X.: Isoprene emissions over Asia 1979-2012: impact of climate and land-use changes, Atmos. Chem. Phys., 14, 4587-4605, 10.5194/acp-14-4587-2014, 2014.

Unger, N.: On the role of plant volatiles in anthropogenic global climate change, Geophys. Res. Lett., 41, 8563-8569, 10.1002/2014GL061616, 2014a.

Unger, N.: Human land-use-driven reduction of forest volatiles cools global climate, Nat. Clim. Change, 4, 907-910, 10.1038/nclimate2347,
500 2014b.

Volkamer, R., Jimenez, J. L., San Martini, F., Dzepina, K., Zhang, Q., Salcedo, D., Molina, L. T., Worsnop, D. R., and Molina, M. J.: Secondary organic aerosol formation from anthropogenic air pollution: Rapid and higher than expected, Geophys. Res. Lett., 33, 10.1029/2006GL026899, 2006.

Wang, H., Wu, Q., Liu, H., Wang, Y., Cheng, H., Wang, R., Wang, L., Xiao, H., and Yang, X.: Sensitivity of biogenic volatile organic
505 compound emissions to leaf area index and land cover in Beijing, Atmos. Chem. Phys., 18, 9583-9596, 10.5194/acp-18-9583-2018, 2018a.

Wang, H., Wu, Q., Guenther, A. B., Yang, X., Wang, L., Xiao, T., Li, J., Feng, J., Xu, Q., and Cheng, H.: A long-term estimation of biogenic volatile organic compound (BVOC) emission in China from 2001–2016: the roles of land cover change and climate variability, Atmos. Chem. Phys., 21, 4825-4848, 10.5194/acp-21-4825-2021, 2021.

Wang, L., Jang, C., Zhang, Y., Wang, K., Zhang, Q., Streets, D., Fu, J., Lei, Y., Schreifels, J., He, K., Hao, J., Lam, Y.-F., Lin, J., Meskhidze,
510 N., Voorhees, S., Evarts, D., and Phillips, S.: Assessment of air quality benefits from national air pollution control policies in China. Part I: Background, emission scenarios and evaluation of meteorological predictions, Atmos. Environ., 44, 3442-3448, https://doi.org/10.1016/j.atmosenv.2010.05.051, 2010.

Wang, P., Ying, Q., Zhang, H., Hu, J., Lin, Y., and Mao, H.: Source apportionment of secondary organic aerosol in China using a regional source-oriented chemical transport model and two emission inventories, Environ. Pollut., 237, 756-766,
515 https://doi.org/10.1016/j.envpol.2017.10.122, 2018b.

Wang, P., Chen, Y., Hu, J., Zhang, H., and Ying, Q.: Source apportionment of summertime ozone in China using a source-oriented chemical transport model, Atmos. Environ., 211, 79-90, https://doi.org/10.1016/j.atmosenv.2019.05.006, 2019.

Wang, P., Chen, K., Zhu, S., Wang, P., and Zhang, H.: Severe air pollution events not avoided by reduced anthropogenic activities during COVID-19 outbreak, Resources, Conservation and Recycling, 158, 104814, https://doi.org/10.1016/j.resconrec.2020.104814, 2020a.

520 Wang, R., Bei, N., Wu, J., Li, X., Liu, S., Yu, J., Jiang, Q., Tie, X., and Li, G.: Cropland nitrogen dioxide emissions and effects on the ozone pollution in the North China plain, Environ. Pollut., 294, 118617, https://doi.org/10.1016/j.envpol.2021.118617, 2022.

Wang, Y., Zhao, Y., Zhang, L., Zhang, J., and Liu, Y.: Modified regional biogenic VOC emissions with actual ozone stress and integrated land cover information: A case study in Yangtze River Delta, China, Sci. Total. Environ., 727, 10.1016/j.scitotenv.2020.138703, 2020b.

Wu, K., Yang, X., Chen, D., Gu, S., Lu, Y., Jiang, Q., Wang, K., Ou, Y., Qian, Y., Shao, P., and Lu, S.: Estimation of biogenic VOC
525 emissions and their corresponding impact on ozone and secondary organic aerosol formation in China, Atmos. Res., 231, 104656, https://doi.org/10.1016/j.atmosres.2019.104656, 2020.

Xiao, Z., Liang, S., Wang, J., Chen, P., Yin, X., Zhang, L., and Song, J.: Use of General Regression Neural Networks for Generating the GLASS Leaf Area Index Product From Time-Series MODIS Surface Reflectance, IEEE Trans Geosci. Remote Sens., 52, 209-223, 10.1109/TGRS.2013.2237780, 2014.

530 Xiao, Z., Liang, S., Wang, J., Xiang, Y., Zhao, X., and Song, J.: Long-Time-Series Global Land Surface Satellite Leaf Area Index Product Derived From MODIS and AVHRR Surface Reflectance, IEEE Trans Geosci. Remote Sens., 54, 5301-5318, 10.1109/TGRS.2016.2560522, 2016.

Yang, F., Yang, J., Wang, J., and Zhu, Y.: Assessment and Validation of MODIS and GEOV1 LAI With Ground-Measured Data and an Analysis of the Effect of Residential Area in Mixed Pixel, IEEE Journal of Selected Topics in Applied Earth Observations and Remote
535 Sensing, 8, 763-774, 10.1109/JSTARS.2014.2340452, 2015.

Ying, Q., and Krishnan, A.: Source contributions of volatile organic compounds to ozone formation in southeast Texas, J. Geophys. Res. Atmos., 115, https://doi.org/10.1029/2010JD013931, 2010.

Ying, Q., Li, J., and Kota, S. H.: Significant Contributions of Isoprene to Summertime Secondary Organic Aerosol in Eastern United States, Environ. Sci. Technol., 49, 7834-7842, 10.1021/acs.est.5b02514, 2015.

540 Zhang, H., and Ying, Q.: Secondary organic aerosol formation and source apportionment in Southeast Texas, Atmos. Environ., 45, 3217-3227, https://doi.org/10.1016/j.atmosenv.2011.03.046, 2011.

Zhang, H., Li, J., Ying, Q., Yu, J. Z., Wu, D., Cheng, Y., He, K., and Jiang, J.: Source apportionment of $PM_{2.5}$ nitrate and sulfate in China using a source-oriented chemical transport model, Atmos. Environ., 62, 228-242, https://doi.org/10.1016/j.atmosenv.2012.08.014, 2012.

Zhang, R., Cohan, A., Biazar, A. P., and Cohan, D. S.: Source apportionment of biogenic contributions to ozone formation over the United
545 States, Atmos. Environ., 164, 8-19, 10.1016/j.atmosenv.2017.05.044, 2017.

Zhang, X., Cappa, C. D., Jathar, S. H., McVay, R. C., Ensberg, J. J., Kleeman, M. J., and Seinfeld, J. H.: Influence of vapor wall loss in laboratory chambers on yields of secondary organic aerosol, Proc. Nat. Acad. Sci., 111, 5802-5807, 10.1073/pnas.1404727111, 2014.

Zhang, Y. L., Zhang, R. X., Yu, J. Z., Zhang, Z., Yang, W. Q., Zhang, H. N., Lyu, S. J., Wang, Y. S., Dai, W., Wang, Y. H., and Wang, X. M.: Isoprene Mixing Ratios Measured at Twenty Sites in China During 2012-2014: Comparison With Model Simulation, J. Geophys. Res. Atmos., 125, 10.1029/2020JD033523, 2020.

Zhao, C., Wang, Y., Yang, Q., Fu, R., Cunnold, D., and Choi, Y.: Impact of East Asian summer monsoon on the air quality over China: View from space, Journal of Geophysical Research: Atmospheres, 115, https://doi.org/10.1029/2009JD012745, 2010.

Zhao, C., Huang, M. Y., Fast, J. D., Berg, L. K., Qian, Y., Guenther, A., Gu, D. S., Shrivastava, M., Liu, Y., Walters, S., Pfister, G., Jin, J. M., Shilling, J. E., and Warneke, C.: Sensitivity of biogenic volatile organic compounds to land surface parameterizations and vegetation distributions in California, Geosci. Model Dev., 9, 1959-1976, 10.5194/gmd-9-1959-2016, 2016.

Zhao, H., Chen, K., Liu, Z., Zhang, Y., Shao, T., and Zhang, H.: Coordinated control of PM2.5 and O3 is urgently needed in China after implementation of the "Air pollution prevention and control action plan", Chemosphere, 270, 129441, https://doi.org/10.1016/j.chemosphere.2020.129441, 2021.

Zheng, B., Huo, H., Zhang, Q., Yao, Z. L., Wang, X. T., Yang, X. F., Liu, H., and He, K. B.: High-resolution mapping of vehicle emissions in China in 2008, Atmos. Chem. Phys., 14, 9787-9805, 10.5194/acp-14-9787-2014, 2014.

Zhu, S., Poetzscher, J., Shen, J., Wang, S., Wang, P., and Zhang, H.: Comprehensive Insights Into O3 Changes During the COVID-19 From O3 Formation Regime and Atmospheric Oxidation Capacity, Geophys. Res. Lett., 48, e2021GL093668, https://doi.org/10.1029/2021GL093668, 2021.

565

0 — Bare Vegetation   5 — Broadleaf Evergreen Temperate Tree   10 — Broadleaf Deciduous Temperate Shrub

1 — Needleleaf Evergreen Temperate Tree   6 — Broadleaf Deciduous Tropical Tree   11 — Broadleaf Deciduous Boreal Shrub

2 — Needleleaf Evergreen Boreal Tree   7 — Broadleaf Deciduous Temperate Tree   12 — Grass

3 — Needleleaf Deciduous Boreal Tree   8 — Broadleaf Deciduous Boreal Tree   13 — Crop

4 — Broadleaf Evergreen Tropical Tree   9 — Broadleaf Evergreen Temperate Shrub   14 — Ocean

Figure 1. Simulation domain with the spatial distribution of major PFTs in each grid.

570
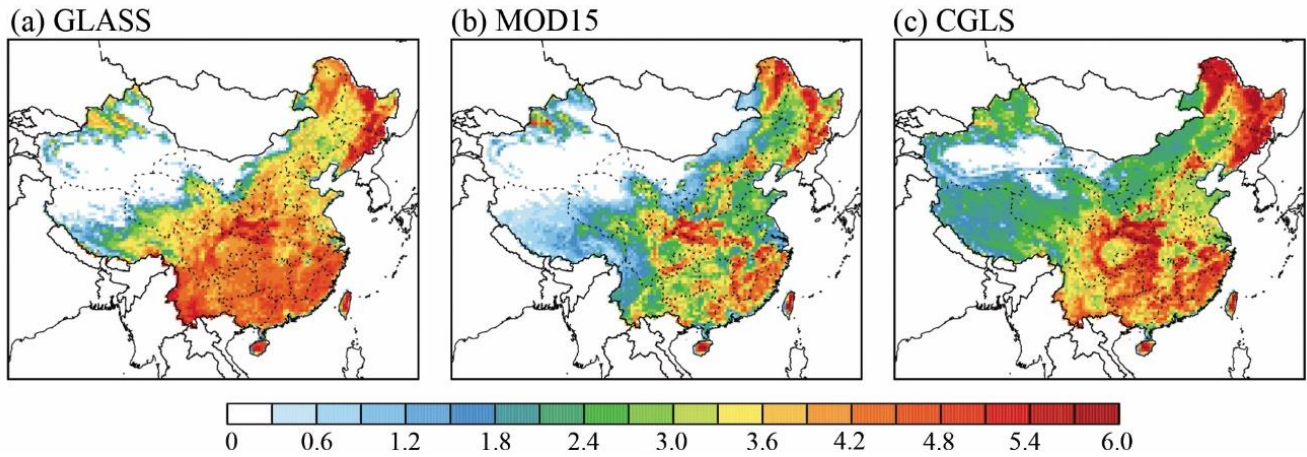
Figure 2. Distribution of LAIv from different satellite datasets in the summer of 2016.
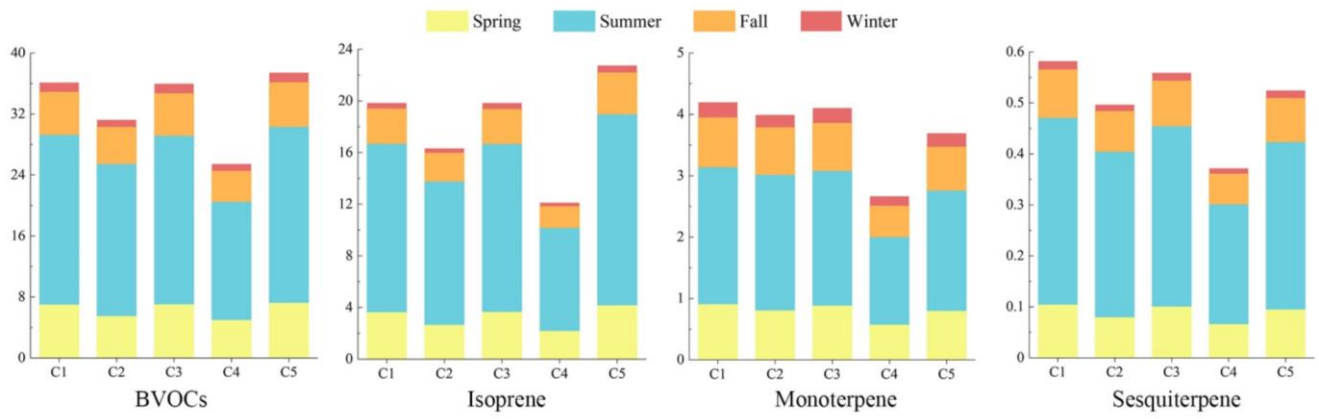
575

Figure 3. Seasonal emissions of isoprene, monoterpenes, sesquiterpenes, and total BVOCs of each case in China. Unit is Tg.
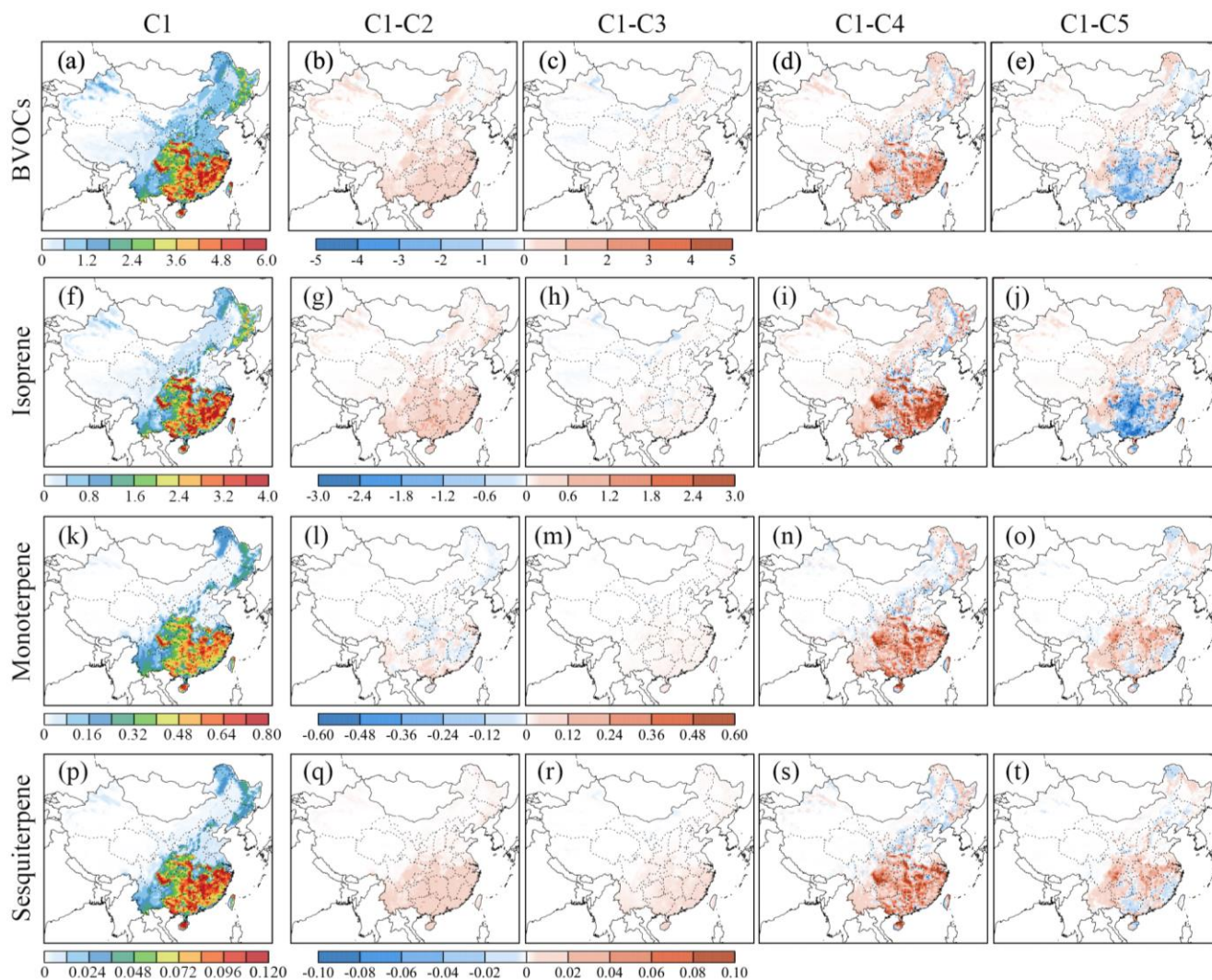
Figure 4. Comparison of three main BVOC species in different cases in summer (June, July and August) ((a), (f), (k), and (p): C1; (b), (g), (l), and (q): C1-C2; (c), (h), (m), and (r): C1-C3; (d), (i), (n), and (s): C1-C4; (e), (j), (o), and (t): C1 -C5). Unit is mg m^{-2} h^{-1}.
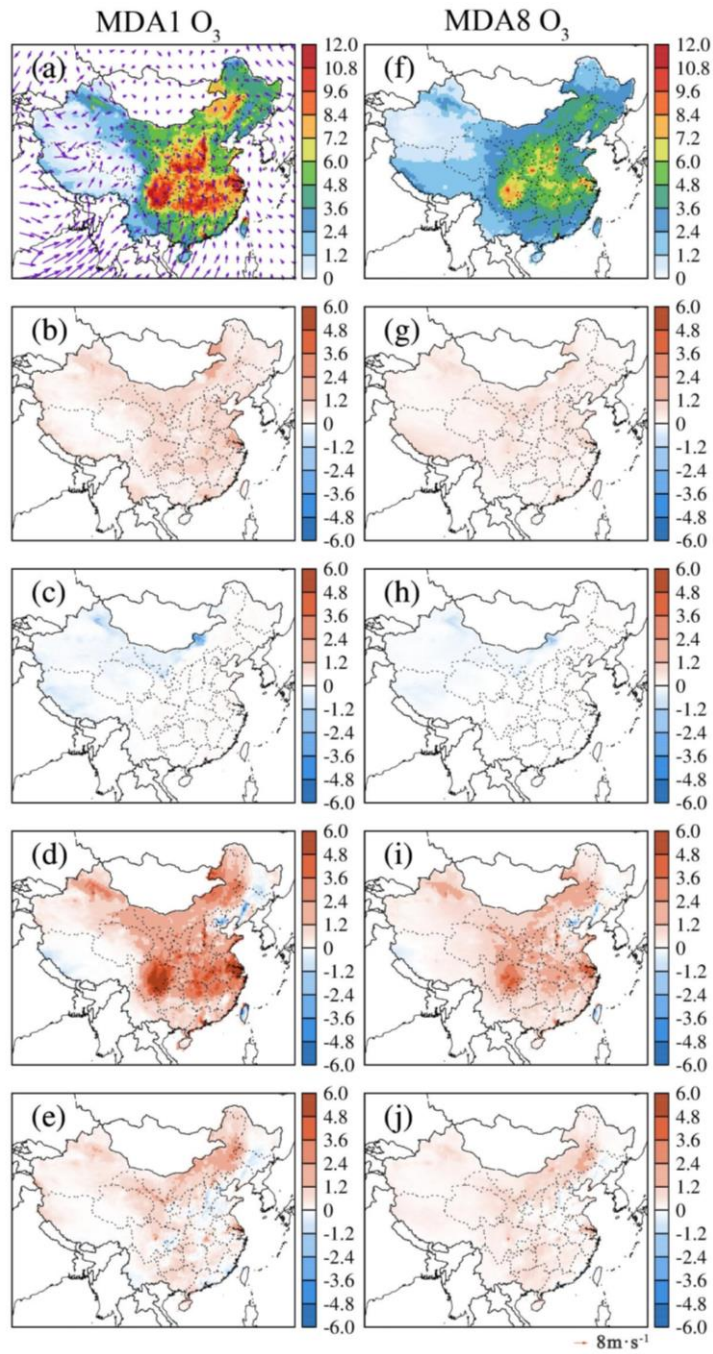
Figure 5. Spatial distributions of MDA1 O₃ and MDA8 O₃ from biogenic source in different cases in summer ((a) and (f): C1, (b) and (g): C1-C2, (c) and (h): C1-C3, (d) and (i): C1-C4, (e) and (j): C1-C5). Unit is ppb.
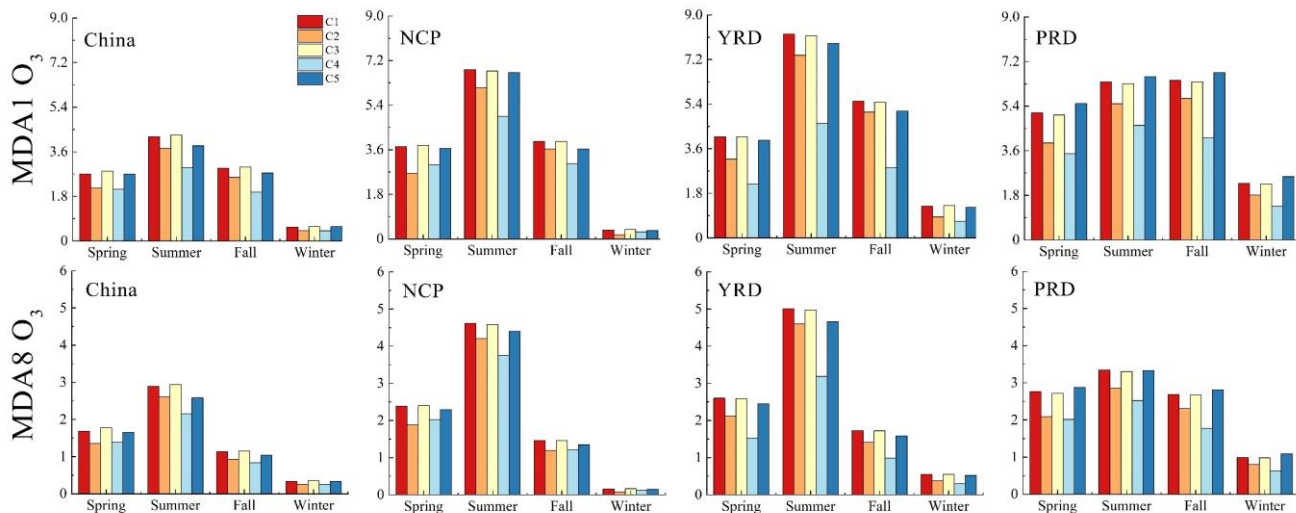
Figure 6. Seasonal averaged concentrations of MDA1 O_3 and MDA8 O_3 from biogenic emissions in important regions and China.
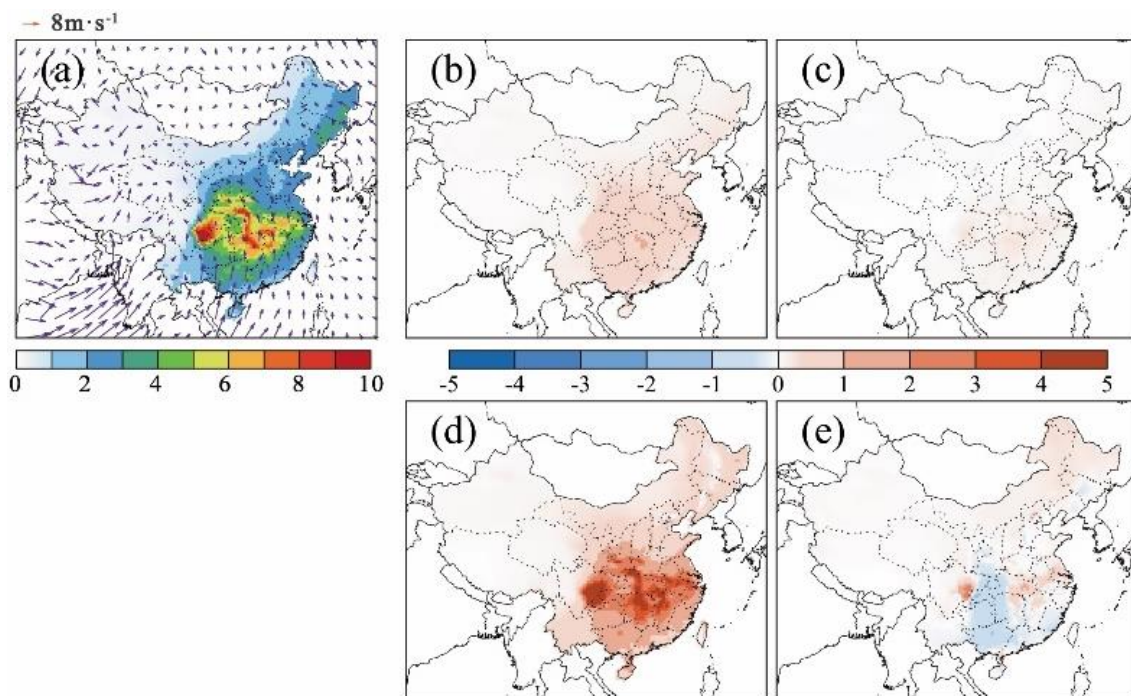
Figure 7. Spatial distributions of simulated SOA from biogenic source in different cases in summer. Unit is μg m^{-3} ((a): C1, (b): C1-C2, (c): C1-C3, (d): C1-C4, (e): C1-C5).
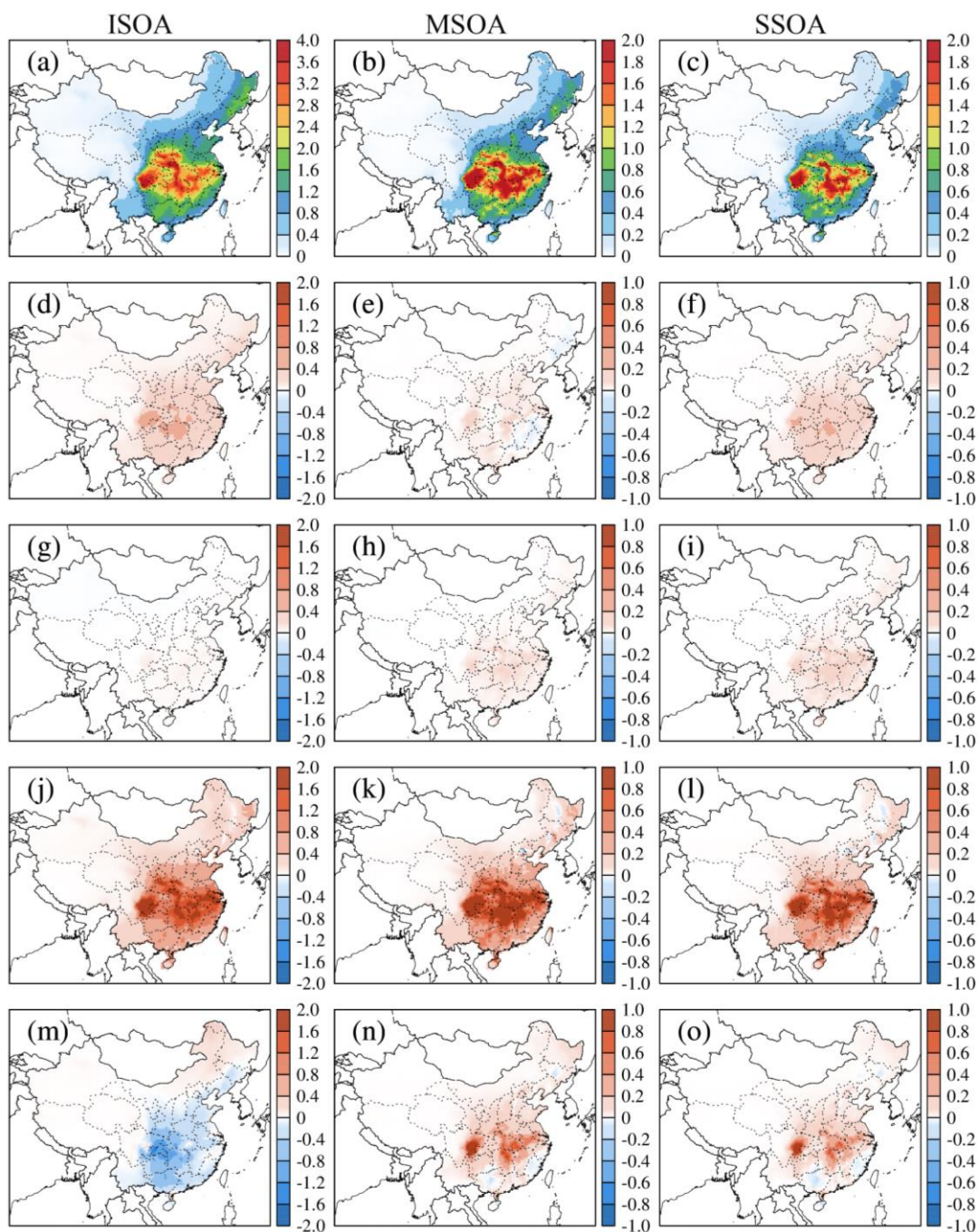
Figure 8. Spatial distributions of simulated SOA from isoprene (ISOA), monoterpenes (MSOA), and sesquiterpenes (SSOA) in different cases in summer ((a), (b), and (c): C1; (d), (e), and (f): C1-C2; (g), (h), and (i): C1-C3; (j), (k), and (l): C1-C4; (m), (n), and (o): C1-C5). Unit is μg m⁻³.
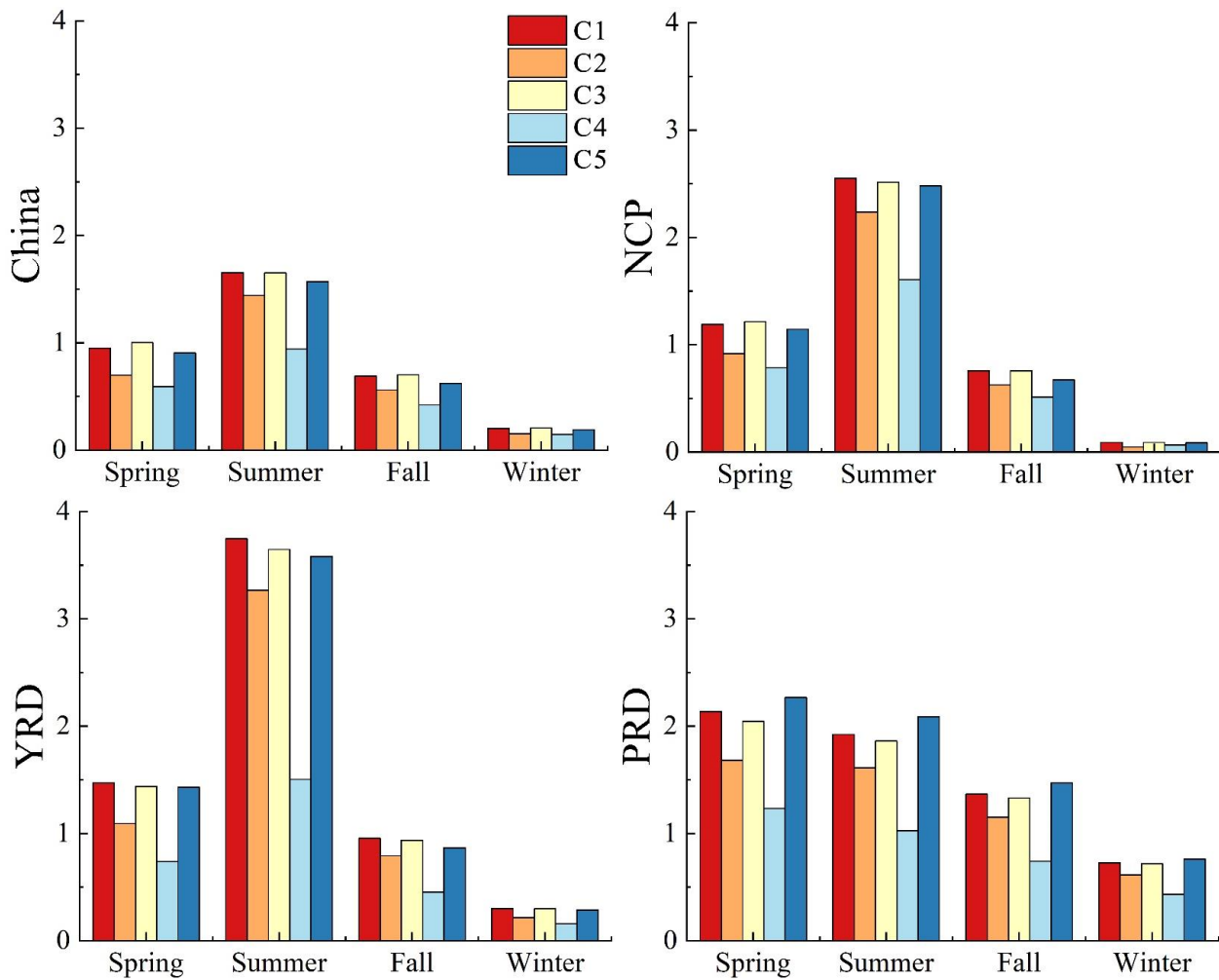
600 **Figure 9. Seasonal distributions of biogenic SOA (BSOA) for all cases in important regions and China. Unit is μg m⁻³.**

Table 1. Simulation schemes with different land cover (LC) and leaf area index (LAI).

| Case | BVOCs | | Description |
	LC	LAI	
C1	MCD12Q1	GLASS	As baseline
C2	MCD12Q1	MOD15	Compared to C1, accounts for LAI difference between GLASS and MOD15
C3	MCD12Q1	CGLS	Compared to C1, accounts for LAI difference between GLASS and CGLS
C4	C3S LC	GLASS	Compared to C1, accounts for LC difference between MCD12Q1 and C3S LC
C5	CGLS LC	GLASS	Compared to C1, accounts for LC difference between MCD12Q1 and CGLS LC

605 **Table 2. Estimated BVOC emissions (Tg) in different cases across China.**

	C1	C2	C3	C4	C5
Isoprene	19.84	16.32	19.83	12.10	22.73
Monoterpenes	4.19	3.99	4.10	2.66	3.69
Sesquiterpenes	0.58	0.50	0.56	0.37	0.52
Other BVOCs	11.49	10.42	11.46	10.29	10.45
Total	36.10	31.22	35.94	25.42	37.39

Table 3. Previous studies of BVOC emissions estimated using MEGAN in China, unit is Tg yr^{-1}.

Reference	Year	LAI	PFT	Isoprene	Monoterpenes	Total BVOCs
Wang et al. (2021)	2016	MODIS MOD15A2H	MODIS MCD12C1	16.70	4.12	35.48
Wu et al. (2020)	2017	MODIS MOD15A2H	MODIS MCD12Q1	13.30	3.09	23.54
Li et al. (2020)	2018	MEGAN-L database	Vegetation Atlas	37.45	6.69	58.89
Stavrakou et al. (2014)	1979-2012	MODIS MOD15A2H	Default MEGAN map with the updated cropland map	9.30	\	\
Li et al. (2013)	2003	Biomass-apportion models results	Vegetation Atlas	20.70	4.90	42.50
Fu and Liao (2012)	2001-2006	MODIS MOD15A2H	MODIS MCD12Q1	9.59	2.83	18.85